AERE - R 8925

United Kingdom Atomic Energy Authority

HARWELL

Calibration of the Harwell linac mark II total scattering spectrometer

P.A.V. Johnson, A.C. Wright, R.N. Sinclair
Materials Physics Division
AERE Harwell, Oxfordshire
January 1978

PRICE £1.00 net from H.M. Stationery Office

CALIBRATION OF THE HARWELL LINAC MARK II TOTAL SCATTERING SPECTROMETER

P.A.V. Johnson[+]
A.C. Wright[+]
R.N. Sinclair*

ABSTRACT

A calibration is presented for the Harwell linac mark II total scattering spectrometer based on nickel powder diffraction data. It is found that the initial delay is wavelength (λ) dependent and may be expressed as a power series in λ. Two sets of calibration constants are given appropriate to the truncation of this series respectively at the linear and quadratic terms. In the case of the linear fit the overall accuracy of the momentum transfer scale is better than ~0.5%.

[+]J.J. Thomson Physical Laboratory, Whiteknights, Reading, Berks., RG6 2AF, U.K.

*Materials Physics Division,
A.E.R.E., HARWELL.

January 1978

HL.78/51
HMD.

CONTENTS

TABLES

ILLUSTRATIONS

ISBN 0 - 70 - 580488 - 7

1. Introduction

In recent years, there has been considerable activity in the development of time of flight diffraction methods using pulsed neutron sources. This technique has a number of advantages over reactor methods, particularly for amorphous materials, where the increased real space resolution is of great importance. The present report describes the calibration of the improved version of the total scattering spectrometer on the Harwell electron linear accelerator (linac). Details of the earlier instrument and some experiments performed on it can be found in a paper by Sinclair et al.[1] The current spectrometer is also designed specifically for the study of amorphous materials and its layout is shown schematically in Figure 1.

The linear accelerator is used to inject short pulses of 45 MeV electrons into a water-cooled uranium target where fast neutrons are generated by (γ,n) and (γ,f) reactions. The neutrons are moderated by a slab of polyethylene and pass on through a tapered collimator in the shielding wall. The new spectrometer has a six position sample changer and six fixed counter angles in place of the previous four. Collimation is provided by the sample size and a slit in the boron carbide loaded shielding in front of each of the lower angle detectors. The backward angle (150°) detector (detector 1) consists of a bank of six counters arranged so as to lie on a time focussing locus.[2] In order to increase the count rate for the lower angle detectors, counters are placed symmetrically on each side of the beam line, the scattering angles being matched to within 0.1 of a resolution width. Both the incident and downstream neutron beams are monitored by fission chambers.

For elastic neutron scattering, the magnitude of the scattering vector $\underline{Q}$ is given by

$$Q = \frac{4\pi \sin\theta}{\lambda} \qquad (1)$$

where λ is the neutron wavelength and 2θ the scattering angle. If the neutron time of flight over a path length L, from moderator to detector, is τ, then it follows that

$$Q = \frac{4\pi m_n L \sin\theta}{h\tau} \qquad (2)$$

m_n being the neutron mass.

The time of flight is measured by means of a multishot time of flight system. Each detector pulse is tested with a low level discriminator and subsequently fed to a time of flight scaler linked to a Digital

Equipment Corporation GT40 computer display system. The scaler is started by a delayed signal from the linac and the data from each detector is stored as a 2048 × 2 μs channel time of flight spectrum. Thus if a neutron is recorded in a channel n, the time in μs from the start of the time of flight scaler to the channel centre is given by

$$t = 2n - 1 \tag{3}$$

The absolute time of flight τ is simply related to t by

$$\tau = t + D \tag{4}$$

where D is the initial delay. The main part of the initial delay is electronic but there is also a smaller contribution from the time spent by the neutron in traversing the moderator. Hence in order to calculate a Q scale for each detector, it is necessary to know the values of L $\sin\theta$ and D. These quantities were determined by calibration using a standard nickel powder sample and a piece of hafnium foil in the flight path, the resonance of which can be used as an energy marker at short time of flight.

2. Calibration

The nickel powder sample used was contained in a thin walled aluminium can. The resulting diffraction patterns were corrected for background and divided by the scattering from a vanadium standard to approximately remove the effect of the incident spectrum, and are shown in Fig. 2. From Bragg's law

$$Q = \frac{4\pi m_n L \sin\theta}{h(t + D)} = \frac{2\pi}{d_{hk\ell}} \tag{5}$$

which for the (hkℓ) reflection from a cubic material of lattice parameter a becomes

$$\frac{4\pi m_n L \sin\theta}{h(t + D)} = \frac{2\pi\sqrt{h^2 + k^2 + \ell^2}}{a} = \frac{2\pi N_{hk\ell}}{a}$$

and on rearranging

$$t = \frac{1}{N_{hk\ell}}\left[\frac{2m_n a L \sin\theta}{h}\right] - D \tag{6}$$

The observed time of flight is thus a linear function of the reciprocal of $N_{hk\ell}$ from which the product L $\sin\theta$ and the initial delay can be determined. It is not possible to directly separate L and $\sin\theta$. L has to be calculated from the product using the nominal value of 2θ taken from the design specifications of the spectrometer. This value of L together with the position of the hafnium resonance t_R can be used to calculate another value for the initial delay D_R and hence check for consistency at short time (t ~90 μs) where the Bragg reflections are continuous.

$$D = L\sqrt{\frac{m_n}{2E}} - t \qquad (7)$$

The powder patterns were indexed and only distinct or adequately resolved peaks were chosen for the calibration. The Maxwellian component in the incident neutron spectrum gives rise to asymmetric peak profiles, particularly for the higher angle detectors. The centre of the peak at half area t_A is therefore probably a better criterion for the median than the centre of the peak width at half height t_W. Unfortunately, as a result of overlap, the half areas of only a few of the peaks could be determined for each detector. Where possible, the half area positions of the hand smoothed peaks were obtained by continuous summation using Simpson's rule. The shift to higher times δt, relative to the centre of the peak width at half height, is small, amounting to a maximum of about 1 channel (2 μs) for detector 1 and progressively less for those at lower angles. The results are shown in Table 1. Within the error, δt is a constant for each detector and will thus appear as a systematic error in D when formula (6) is used with t_W values.

A linear least squares fit of the form

$$t_W = \frac{A}{N_{hk\ell}} - C \qquad (8)$$

was performed for detector 1, the results of which are shown in Tables 2 and 4. The parameter C represents the least squares estimate of the initial delay D. L $\sin\theta$ can be simply obtained from A

$$L\sin\theta = \frac{hA}{2m_n a} \qquad (9)$$

It can be seen that the agreement between C and D_R is poor. Also the distribution of the difference values t_W (obs – cal) is not random, suggesting that additional terms dependent upon $1/N_{hk\ell}$ would

improve the fit. In the derivation of formula (6) it was assumed that the initial delay was a constant over the time of flight scale. This however, is an approximation, since it is known that the moderator part of the initial delay is wavelength dependent.[3] A better expression for the observed time would therefore be

$$t = \frac{1}{N_{hk\ell}}\left[\frac{2m_n\, a\, L \sin\theta}{h}\right] - D(\lambda) \tag{10}$$

$D(\lambda)$ is a slowly varying function and can be satisfactorily expanded as a polynomial in λ

$$D(\lambda) = D_o + D_1\lambda + D_2\lambda^2 ..... + D_n\lambda^n \tag{11}$$

For the Bragg reflections

$$\lambda = \frac{2a \sin\theta}{N_{hk\ell}} \tag{12}$$

Substituting for λ and taking $D(\lambda)$ to the second order term gives

$$t = \frac{1}{N_{hk\ell}}\left[\frac{2m_n a\, L \sin\theta}{h}\right] - D_o - \frac{2D_1 a \sin\theta}{N_{hk\ell}} - \frac{4D_2 a^2 \sin^2\theta}{N_{hk\ell}^2} \tag{13}$$

On further rearrangement, the constant D_1 can be incorporated into an effective flight path length L'.

$$t = \frac{1}{N_{hk\ell}}\left[\frac{2am_n\, L' \sin\theta}{h}\right] - \frac{1}{N_{hk\ell}^2}\left[4D_2 a^2 \sin^2\theta\right] - D_o \tag{14}$$

$$L' = L - \frac{D_1 h}{m_n} \tag{15}$$

A similar treatment for energy gives

$$t = L'\sqrt{\frac{m_n}{2E}} - D_o - \frac{D_2 h^2}{2Em_n} \tag{16}$$

For energies close to the Hf resonance, the second term in (16) amounts to less than 0.05 μs and so can

be neglected in the calculation of D_o. There is marked improvement when a fit of the form

$$t_W = \frac{A}{N_{hk\ell}} - \frac{B}{N_{hk\ell}^2} - C \qquad (17)$$

is used. In both the linear and quadratic least squares fits, the observations were given unit weight. Quadratic fits were obtained for detectors 1 to 3. Only three reflections could be used for the detectors 4 and 5 and so it was necessary to resort to a linear fit. Since B is a function of $\sin^2\theta$, its value will decrease rapidly with decreasing 2θ and the effect on the low angle counters should be small. The difference distribution for detector 4 suggests that there is still a small quadratic component present. The linear fit to detector 5 is excellent but the small errors are probably fortuitous. The resolution of detector 6 is so poor that no peaks could be used for calibration. In this case averages of the initial delays and flight path lengths for detectors 2 to 5 are probably the best values to use. The positions of the hafnium resonances have been quoted in Table 2 for detectors 2 and 3. The resonance profiles however, were distorted by interference with peaks and the values of D_R are not reliable.

The parameters for detector 1, although self consistent, show a significant difference from the others. This is not very surprising in view of the special nature of this detector and also the fact that the output passes through a different chain of electronics.

The inclusion of the second order term in (14) modifies formula (2) from which Q is calculated. Re-expressing (14) in terms of Q

$$t = \frac{1}{Q}\left[\frac{4\pi m_n L' \sin\theta}{h}\right] - \frac{1}{Q^2}\left[16\pi^2 D_2 \sin^2\theta\right] - D_o \qquad (18)$$

If the absolute time of flight is τ_o where

$$\tau_o = t + D_o \qquad (19)$$

then

$$\tau_o = \frac{1}{Q}\left[\frac{4\pi m_n L' \sin\theta}{h}\right] - \frac{1}{Q^2}\left[16\pi^2 D_2 \sin^2\theta\right]$$

and

$$r_o Q^2 - Q\left[\frac{4\pi m_n L' \sin\theta}{h}\right] + 16\pi^2 D_2 \sin^2\theta = 0 \qquad (20)$$

For positive solutions of equation (20)

$$Q = \frac{4\pi m_n L' \sin\theta}{2hr_o} + \frac{\sqrt{\left[\frac{4\pi m_n L' \sin\theta}{h}\right]^2 - 64\pi^2 D_2 \sin^2\theta r_o}}{2r_o}$$

$$Q = \frac{4\pi m_n L' \sin\theta}{2hr_o}\left[1 + \sqrt{1 - \frac{4D_2 r_o h^2}{m_n^2 L'^2}}\right] \qquad (21)$$

Since the term involving r_o inside the square root in equation (21) is very small, the root can be expanded by the binomial theorem to first order with good approximation.

$$\left[1 - \frac{4D_2 r_o h^2}{m_n^2 L'^2}\right]^{1/2} \simeq 1 - \frac{2D_2 r_o h^2}{m_n^2 L'^2} \qquad (22)$$

substituting in (21) gives

$$Q \simeq \frac{4\pi m_n L' \sin\theta}{hr_o} - \frac{4\pi h D_2 \sin\theta}{m_n L'} \qquad (23)$$

In terms of the least squares parameters equations (22) and (23) become

$$Q = \frac{\pi A}{a(t + C)}\left[1 + \sqrt{1 - \frac{4B(t + C)}{A^2}}\right] \qquad (24)$$

and

$$Q \simeq \frac{2\pi A}{a(t + C)} - \frac{2\pi B}{aA} \qquad (25)$$

The approximate formulae above have a maximum error at low Q but even there this is very small. At the lowest value of Q for detector 1, for example, the error is only 0.003%.

3. Optimisation to a Linear Relationship

In data analysis, it is much more convenient to use a formula which assumes a linear initial delay.

$$Q = \frac{4\pi m_n L' \sin\theta}{h r_o} \tag{26}$$

Parameters must thus be found to optimise this formula over the observed Q scale. Fixing D_o as the quadratic least squares value in order to ensure accuracy at high Q.

$$Q_{obs} = \frac{4\pi m_n L'' \sin\theta}{h(t_W + C)} \tag{27}$$

$$Q_{cal} = \frac{2\pi N_{hk\ell}}{a} \tag{28}$$

The optimisation can be performed to suit two different conditions. Accurate positions on the Q scale may be needed or more usually, after Fourier inversion, the precision is required in the bond length determination. In order to deal with those two situations, values of $L'' \sin\theta$ were found such that for n observations, the functions

$$G = \sum_{j=1}^{n} [(Q_{obs})_j - (Q_{cal})_j]^2 \tag{29}$$

$$M = \sum_{j=1}^{n} \frac{[(Q_{obs})_j - (Q_{cal})_j]^2}{(Q_{cal})_j^2} \tag{30}$$

are a minimum. The weighting in the latter condition follows from the fact that $\delta Q/Q$ is a direct measure of the percentage bond length error. The minima are satisfied by

$$(L'' \sin\theta)_G = \frac{h \sum_{j=1}^{n} \frac{(N_{hk\ell})_j}{[(t_W)_j + C]}}{2m_n a \sum_{j=1}^{n} \frac{1}{[(t_W)_j + C]^2}} \tag{31}$$

and

$$(L'' \sin\theta)_M = \frac{h \sum_{j=1}^{n} \frac{1}{(N_{hk\ell})_j [(t_W)_j + C]}}{2m_n a \sum_{j=1}^{n} \frac{1}{(N_{hk\ell})_j^2 [(t_W)_j + C]^2}} \tag{32}$$

The results for each detector are shown in Tables 5-7. $(L'' \sin\theta)_G$ and $(L'' \sin\theta)_M$ are optimum rather than physical parameters and so it is not meaningful to quote errors for them. The error in Q_{obs} is a combination of a systematic error η resulting from using a linear initial delay and a random error ϵ caused by the uncertainty in t. Thus

$$Q_{obs} - Q_{cal} = \delta Q = \eta + \epsilon \tag{33}$$

Over most of the Q scale $\eta >> \epsilon$. The systematic error can be assessed by taking the difference between the optimum linear and quadratic expressions.

$$\eta_G = \frac{4\pi m_n (L'' \sin\theta)_G}{h\tau_o} - \frac{4\pi m_n L' \sin\theta}{2h\tau_o} \left[1 + \sqrt{1 - \frac{4D_2 h^2 \tau_o}{m_n^2 L'^2}} \right] \tag{34}$$

$$\eta_G/Q = \frac{2 (L'' \sin\theta)_G}{L' \sin\theta \left[1 + \sqrt{1 - \frac{4D_2 h^2 \tau_o}{m_n^2 L'^2}} \right]} - 1 \tag{35}$$

Using approximation (23)

$$\eta_G \simeq \frac{4\pi m_n (L'' \sin\theta)_G}{h\tau_o} - \frac{4\pi m_n L' \sin\theta}{h\tau_o} + \frac{4\pi h D_2 \sin\theta}{m_n L'}$$

$$\eta_G(Q_{obs}) \simeq Q_{obs} \left[1 - \frac{L' \sin\theta}{(L'' \sin\theta)_G} \right] + \frac{4\pi h D_2 \sin\theta}{m_n L'} \tag{36}$$

$$\eta_G(Q_{obs})/Q \simeq \frac{Q_{obs}}{Q_{obs}\left[\frac{L' \sin\theta}{(L'' \sin\theta)_G}\right] - \frac{4\pi h D_2 \sin\theta}{m_n L'}} - 1 \qquad (37)$$

The expressions for η_M are similar. Curves for η and η/Q against Q_{obs} have been computed using formulae (34) and (35) and are shown in Figs 3-6 with δQ for the nickel reflections plotted on the same scale. The close agreement of the approximate expressions for η and η/Q to the computed curves, particularly the straight line form of equation (36), can be readily appreciated.

Some idea of the distribution of the random errors ϵ can be obtained from the Q differences for the quadratic or linear fit parameters in the case of the low angle detectors. Assuming a normal distribution, sample standard deviations can be computed and are given in Table 8.

The width ΔQ_{obs} and resolution $\Delta Q_{obs}/Q_{cal}$ of the nickel peaks are shown in Table 9 for optimisation condition G. The parameters in Table 5 can be taken as the best values for the Q scale. An initial delay corrected for the shift to half area, δt, has also been included. As a final check on the calibration, Q scales were computed for the complete nickel powder patterns for each detector. These are shown in Fig. 7 for condition G only, since on this scale no difference can be discerned between the two optimisations.

4. Conclusion

The most interesting feature to arise out of the calibration is the wavelength dependence of the initial delay. For the purposes of this calibration, it was found adequate to truncate a polynomial expansion of the delay at the second order. Reasonable agreement was thus obtained between the values of D_o calculated from the nickel reflections and D_R from the hafnium energy marker. The accuracy of D_o is very dependent on the minimum time of flight to which the position of discrete nickel reflections can be found. Several improvements could be made in this direction in any future calibration of time of flight spectrometers.

If a nickel powder sample is used, it should be contained in a nickel can which eliminates overlapping aluminium peaks. The use of a calibrant with more systematic absences such as germanium has some advantages, but unfortunately valuable reflections are also lost at long time of flight. The problem of not being able to calculate independent values for L and D_R can be overcome by using an additional energy marker such as the beryllium long wavelength cutoff.

In spite of possible improvements, the quality of the overall calibration is good and can be judged from the composite Q plot in Fig. 7. At first sight detector 6 does not seem to agree with the others. This is due however to a combination of the overlapping hafnium resonance and poor resolution giving rise to false features. Using the quoted parameters, bond lengths should be accurate to better than 0.5%.

5. Calibration Constants

Mass of neutron	m_n	$= 1.674920(11) \times 10^{-27}$ Kg
Plancks constant	h	$= 6.626196(50) \times 10^{-34}$ Js
Electron volt	1eV	$= 1.6021917(70) \times 10^{-19}$ J
Cell dimension of nickel	a	$= 3.52387(8) \times 10^{-10}$ m
Hafnium resonance	E_R	$= 1.0964(15)$ eV[4]

References

1. SINCLAIR. R.N., JOHNSON, D.A.G., DORE, J.C., CLARKE, J.H. and WRIGHT, A.C. (1974), Nucl. Instrum. Meth. *117*, 445.

2. CARPENTER, J.M. (1967), Nucl. Instrum. Meth. *47*, 179.

3. CARPENTER, J.M. (1977), Nucl. Instrum. Meth. *145*, 91.

4. MOXON, M.C. (1977), Private Communication.

TABLE 1

Shifts δt for Various Reflections with Means $\overline{\delta t}$ and Standard Deviations

Detector	2θ	(111)	(200)	(220)	(113)	(222)	$\overline{\delta t}$	σ
1	150°	–	1.99	1.88	2.16	2.09	2.03	0.12
2	90°	0.83	1.8	1.22	–	–	1.28	0.49
3	58°	0.37	1.2	–	–	–	0.78	0.59
4	35°	0.42	0.95	–	–	–	0.68	0.37

TABLE 2

Least Squares Parameters for Detectors 1 to 5.

The Position of the Hf Resonance and the Initial Delay D_R are also tabulated

Detector	2θ	B (μs)	D_2 (μs m^{-2})	A (μs)	L′ sinθ (m)	L′(m)	C (μs)	t_R (μs)	D_R (μs)
1	150°	-	-	8171.3 ± 4.5	4.5868 ± 0.0025	4.7486 ± 0.0026	224.6 ± 1.4	96.5 ± 0.5	231.4 ± 0.9
1	150°	85.2 ± 13.3	$1.84 \pm 0.28 \times 10^{20}$	8229.9 ± 9.3	4.620 ± 0.005	4.783 ± 0.005	233.7 ± 1.5	96.5 ± 0.5	233.7 ± 1.1
2	90°	94.0 ± 9.2	$3.78 \pm 0.37 \times 10^{20}$	6081.4 ± 7.3	3.414 ± 0.004	4.828 ± 0.006	243.3 ± 1.3	93.0 ± 0.5	240.3 ± 1.2
3	58°	59.7 ± 15.4	$5.1 \pm 1.3 \times 10^{20}$	4236.0 ± 11.7	2.378 ± 0.006	4.905 ± 0.012	246.4 ± 1.9	93.2 ± 0.5	245.4 ± 1.6
4	35°	-	-	2590.7 ± 7.7	1.454 ± 0.004	4.835 ± 0.013	242.8 ± 3.7	88.5	-
5	20°	-	-	1533.45 ± 0.29	0.86078 ± 0.00016	4.9570 ± 0.0009	241.74 ± 0.14	89.2	-

TABLE 3

Quadratic Least Squares Fits for Detectors 1 to 3

hkℓ	$1/N_{hk\ell}$	$t_{W(obs)}$ μs			$t_{W(cal)}$ μs			$t_{W(obs)} - t_{W(cal)}$ μs		
		150°	90°	58°	150°	90°	58°	150°	90°	58°
111	0.57735	–	3236.6000	2179.1500	–	3236.4770	2179.4047	–	0.1230	-0.2547
200	0.50000	3859.9500	2773.7000	1857.2000	3859.9794	2773.9136	1856.7204	-0.0294	-0.2136	0.4796
220	0.35355	2665.5000	1895.1000	1243.5200	2665.3559	1895.0426	1243.8128	0.1441	0.0574	-0.2928
113	0.30151	2239.9750	1581.5000	–	2239.9748	1581.7709	–	0.0002	-0.2709	–
222	0.28867	2134.8500	1504.8000	–	2134.9482	1504.3981	–	-0.0982	0.4019	–
224	0.20412	1442.2500	–	615.6000	1442.6579	–	615.7952	-0.4078	–	-0.1952
115 333	0.19245	1347.4000	923.5000	566.9000	1347.0089	923.5977	566.6368	0.3911	-0.0977	0.2632

TABLE 4

Linear Least Squares Fits for Detectors 1, 4 and 5

$hk\ell$	$1/N_{hk\ell}$	$t_{W(obs)}$ μs			$t_{W(cal)}$ μs			$t_{W(obs)} - t_{W(cal)}$ μs		
		150°	35°	20°	150°	35°	20°	150°	35°	20°
111	0.57735	–	1252.3500	643.5750	–	1253.0000	643.5997	–	–0.65005	–0.0247
200	0.50000	3859.9500	1053.6000	525.0250	3861.0296	1052.6066	524.9872	–1.0796	0.99338	0.0378
220	0.35355	2665.5000	672.8500	300.4000	2664.3432	673.1933	300.4131	1.1568	–0.34333	–0.0131
113	0.30151	2239.9750	–	–	2239.1089	–	–	0.8660	–	–
222	0.28867	2134.8500	–	–	2134.1895	–	–	0.6605	–	–
224	0.20412	1442.2500	–	–	1443.3064	–	–	–1.05637	–	–
115 333	0.19245	1347.4000	–	–	1347.9473	–	–	–0.54734	–	–

TABLE 5

Optimum Q scale parameters

Detector	2θ	L″sin θ (G) m	L″sin θ (M) m	D μs	$D_{(cor.)}$ μs
1	150°	4.6077	4.6050	233.7	231.7
2	90°	3.3986	3.3942	243.3	242.0
3	58°	2.3695	2.3656	246.4	245.6
4	35°	1.4542	1.4543	242.8	242.1
5	20°	0.8608	0.8608	241.74	241.7
6	10°	(0.4254)	(0.4254)	(243.6)	(243.6)

TABLE 6

Q scale fits for detectors 1 to 3

hkℓ	Q_{cal} Å^{-1}	$t_W + C\mu s$			Min. Condn.	Q_{obs} Å^{-1}			$(Q_{obs} - Q_{cal})$ Å^{-1}			$(Q_{obs} - Q_{cal})/Q_{cal}$		
		150°	90°	58°		150°	90°	58°	150°	90°	58°	150°	90°	58°
111	3.08831	-	3479.900	2425.550	G	-	3.10220	3.10300	-	0.01389	0.01469	-	0.00450	0.00476
					M	-	3.09820	3.09792	-	0.00989	0.00961	-	0.00320	0.00311
200	3.56607	4093.650	3017.000	2103.600	G	3.57529	3.57817	3.57791	0.00922	0.01210	0.01184	0.00259	0.00339	0.00332
					M	3.57324	3.57356	3.57205	0.00717	0.00749	0.00598	0.00201	0.00210	0.00168
220	5.04319	2899.200	2138.400	1489.920	G	5.04828	5.04833	5.05160	0.00510	0.00514	0.00842	0.00101	0.00102	0.00167
					M	5.04539	5.04182	5.04333	0.00221	- 0.00137	0.00014	0.00044	- 0.00027	0.00003
113	5.91366	2473.675	1824.800	-	G	5.91670	5.91591	-	0.00304	0.00225	-	0.00051	0.00038	-
					M	5.91331	5.90828	-	- 0.00035	- 0.00538	-	- 0.00006	- 0.00091	-
222	6.17662	2368.550	1748.100	-	G	6.17930	6.17548	-	0.00269	- 0.00114	-	0.00043	- 0.00018	-
					M	6.17576	6.16751	-	- 0.00085	- 0.00911	-	- 0.00014	- 0.00147	-
224	8.73505	1675.950	-	862.000	G	8.73295	-	8.73142	- 0.00211	-	- 0.00363	- 0.00024	-	- 0.00042
					M	8.72795	-	8.71712	- 0.00711	-	- 0.01793	- 0.00081	-	- 0.00205
115 333	9.26492	1581.100	1166.800	813.300	G	9.25684	9.25210	9.25425	- 0.00809	- 0.01282	- 0.01067	- 0.00087	- 0.00138	- 0.00115
					M	9.25154	9.24017	9.23910	- 0.01339	- 0.02476	- 0.02583	- 0.00144	- 0.00267	- 0.00279

TABLE 7

Q scale fits for detectors 4 and 5

hkℓ	Q_{cal} Å^{-1}	$t_W + C\,\mu s$		Min. Condn.	Q_{obs} Å^{-1}		$(Q_{obs} - Q_{cal})$ Å^{-1}		$(Q_{obs} - Q_{cal})/Q_{cal}$	
		35°	20°		⌣35°	20°	35°	20°	35°	20°
111	3.08831	1495.150	885.315	G	3.08941	3.08836	0.0110	0.00006	0.00036	0.00002
				M	3.08962	3.08838	0.00131	0.00008	0.00042	0.00002
200	3.56607	1296.400	766.765	G	3.56305	3.56586	- 0.00303	- 0.00021	- 0.00085	- 0.00006
				M	3.56328	3.56588	- 0.00279	- 0.00019	- 0.00078	- 0.00005
220	5.04319	915.650	542.140	G	5.04465	5.04330	0.00146	0.00012	0.00029	0.00002
				M	5.04499	5.04333	0.00180	0.00015	0.00036	0.00003

TABLE 8

Standard deviations for the random error in Q_{obs}

Detector	Angle	σQ_{obs}
1	150°	0.0019
2	90°	0.0006
3	58°	0.0028
4	35°	0.0035
5	20°	0.0002

TABLE 9

Width of nickel peaks ΔQ and resolution ΔQ/Q for optimisation condition G

hkℓ	ΔQ_{obs} Å^{-1}					$\Delta Q_{obs} / Q_{cal}$				
	150°	90°	58°	35°	20°	150°	90°	58°	35°	20°
111	-	0.0586	0.0856	0.1325	0.3520	-	0.0190	0.0277	0.0429	0.1140
200	0.0390	0.0702	0.1014	0.1545	0.4047	0.0109	0.0197	0.0284	0.0433	0.1135
220	0.0630	0.1101	0.1544	0.2177	0.5948	0.0125	0.0218	0.0306	0.0432	0.1179
113	0.0779	0.1284	-	-	-	0.0132	0.0217	-	-	-
222	0.0858	0.1357	-	-	-	0.0140	0.0220	-	-	-
224	0.1303	-	0.2370	-	-	0.0149	-	0.0271	-	-
115 333	0.1510	0.1999	0.2640	-	-	0.0163	0.0216	0.0285	-	-

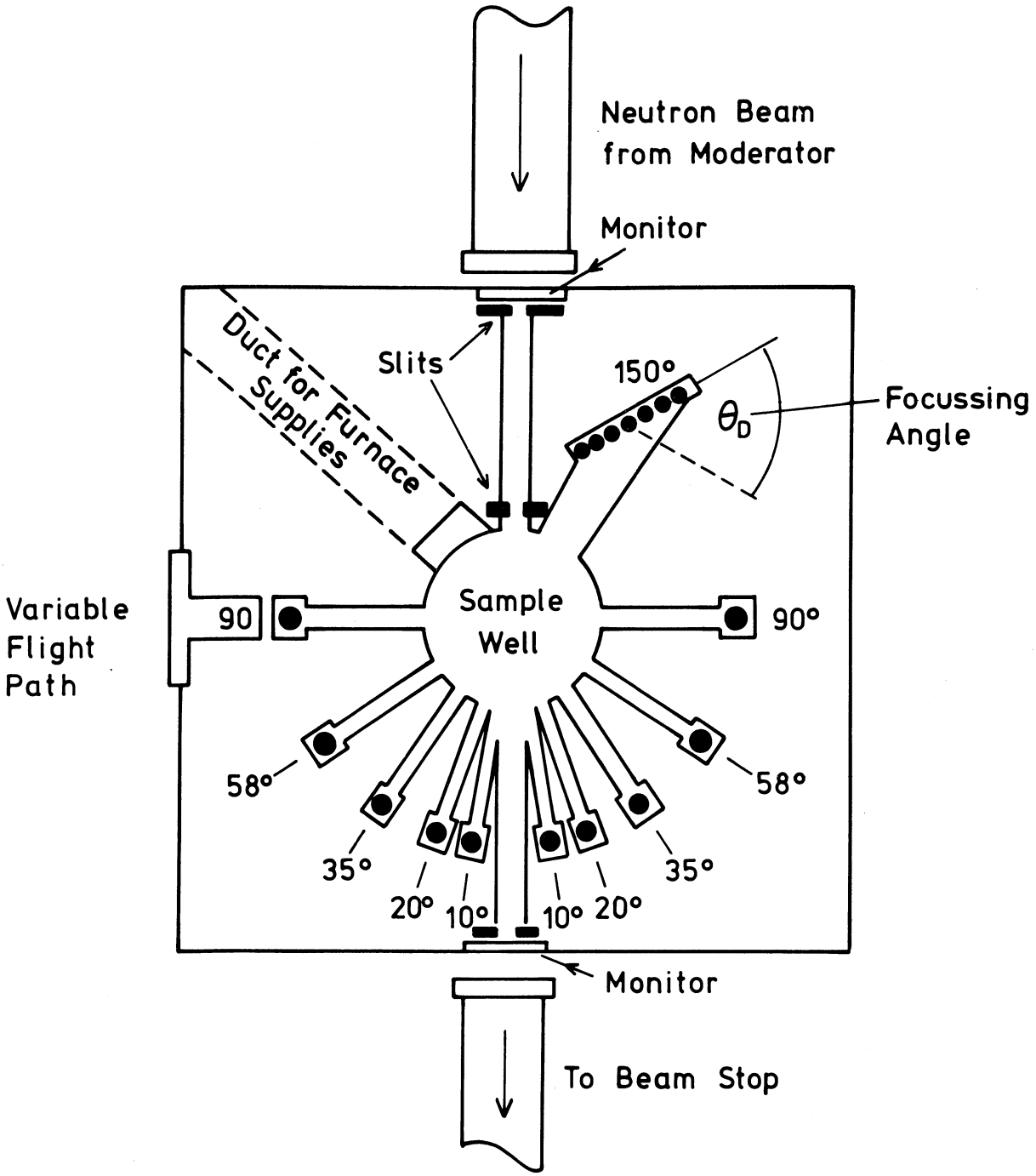

AERE - R 8925 Fig. 1

Experimental layout of the mark II total scattering spectrometer.

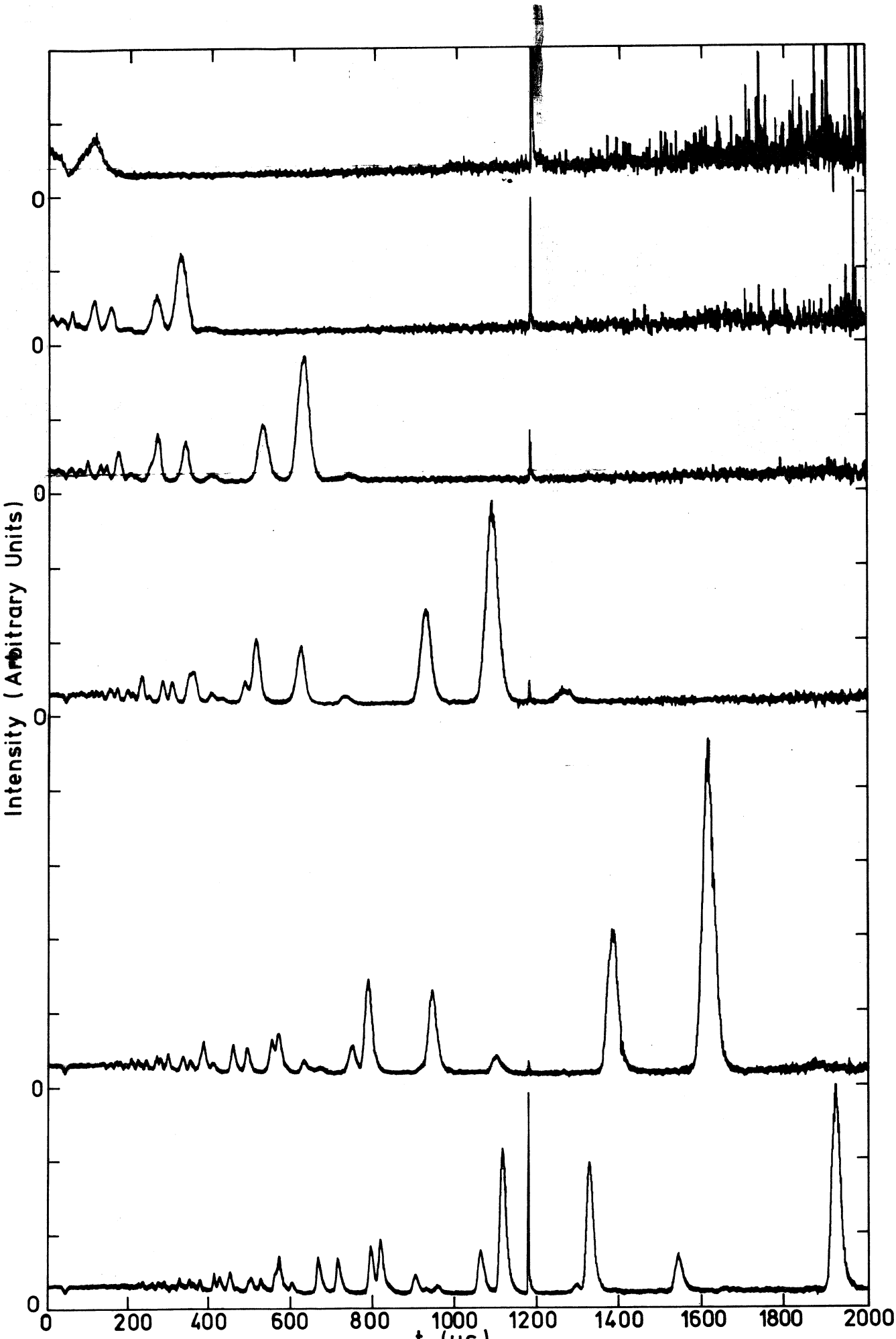

AERE-R8925 FIG. 2

NICKEL POWDER TIME OF FLIGHT SPECTRA FOR DETECTORS 1 TO 6

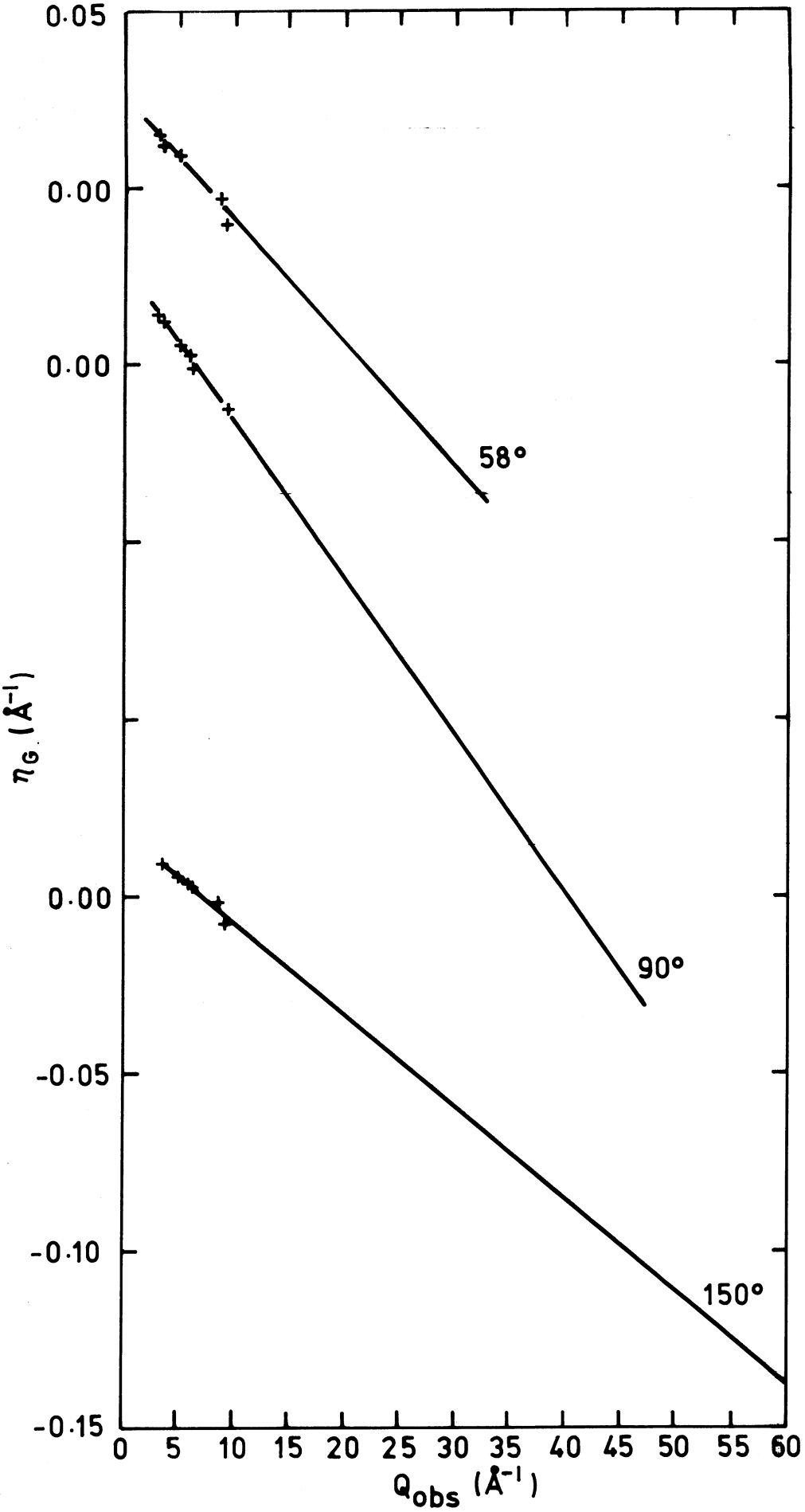

AERE-R8925 FIG 3

PLOT OF THE SYSTEMATIC ERROR η_G AGAINST Q_{obs}

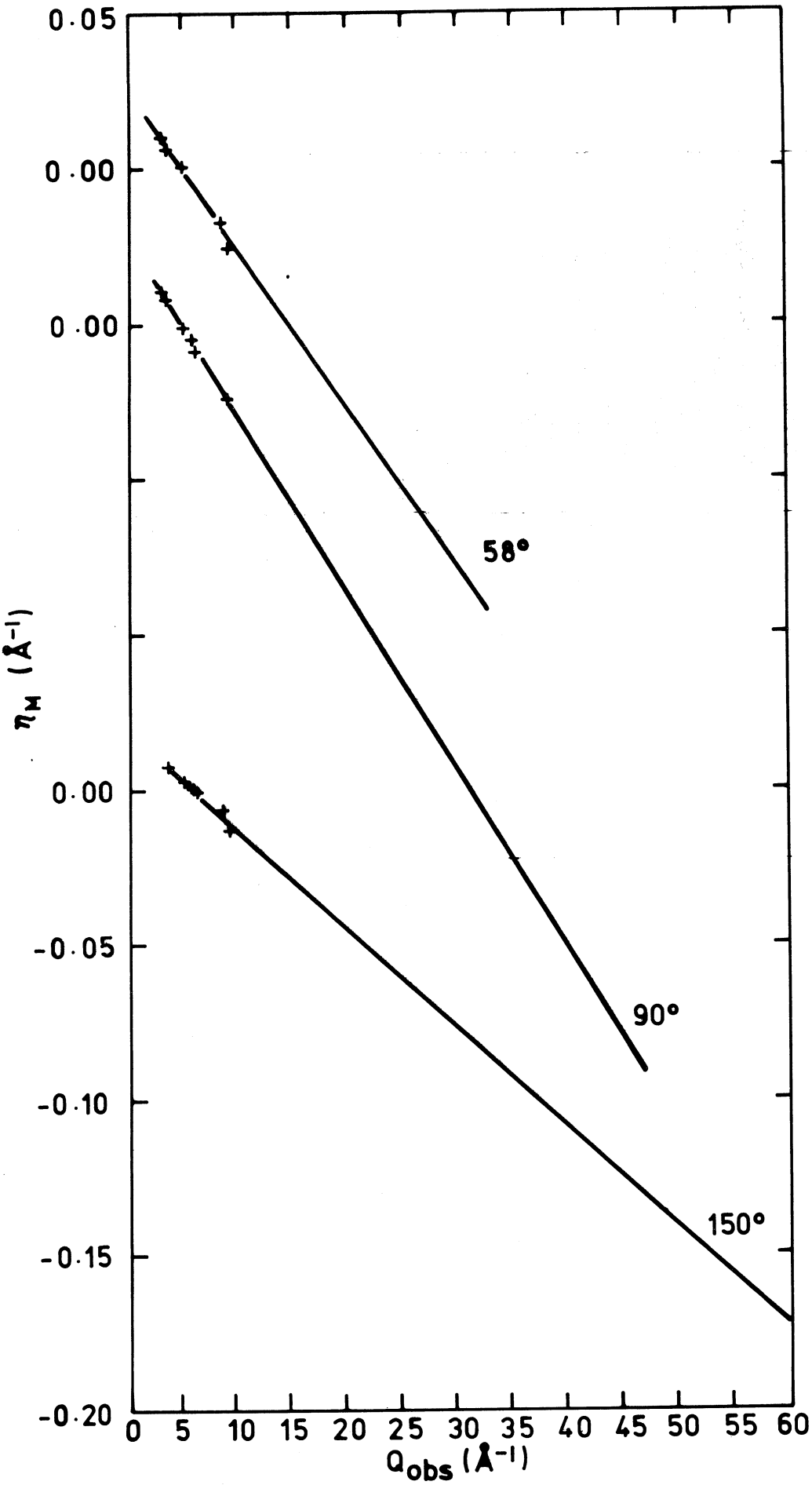

AERE-R8925 FIG. 4

PLOT OF THE SYSTEMATIC ERROR η_M AGAINST Q_{obs}.

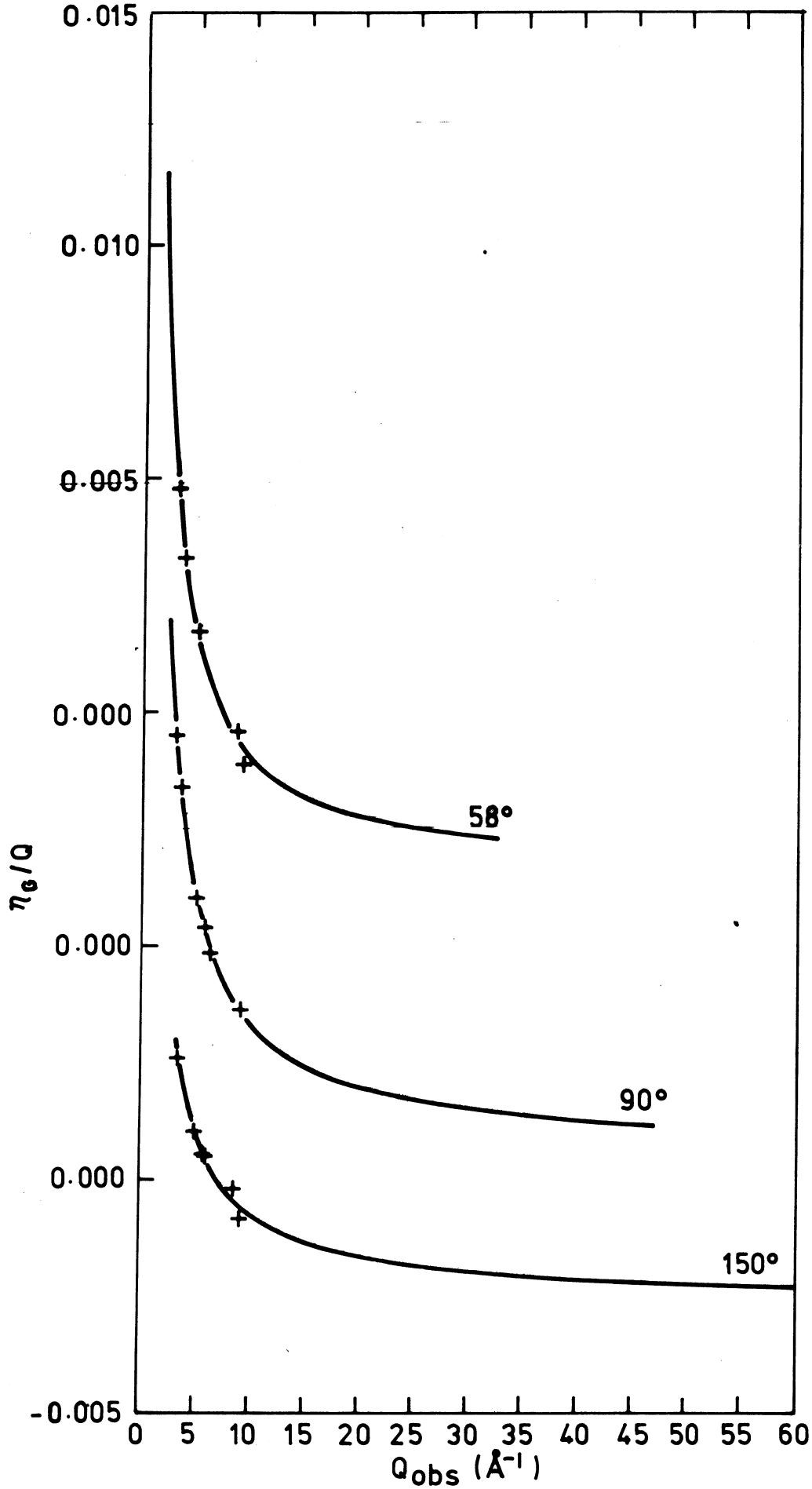

AERE R8925 FIG.5

PLOT OF η_G/Q AGAINST Q_{obs}

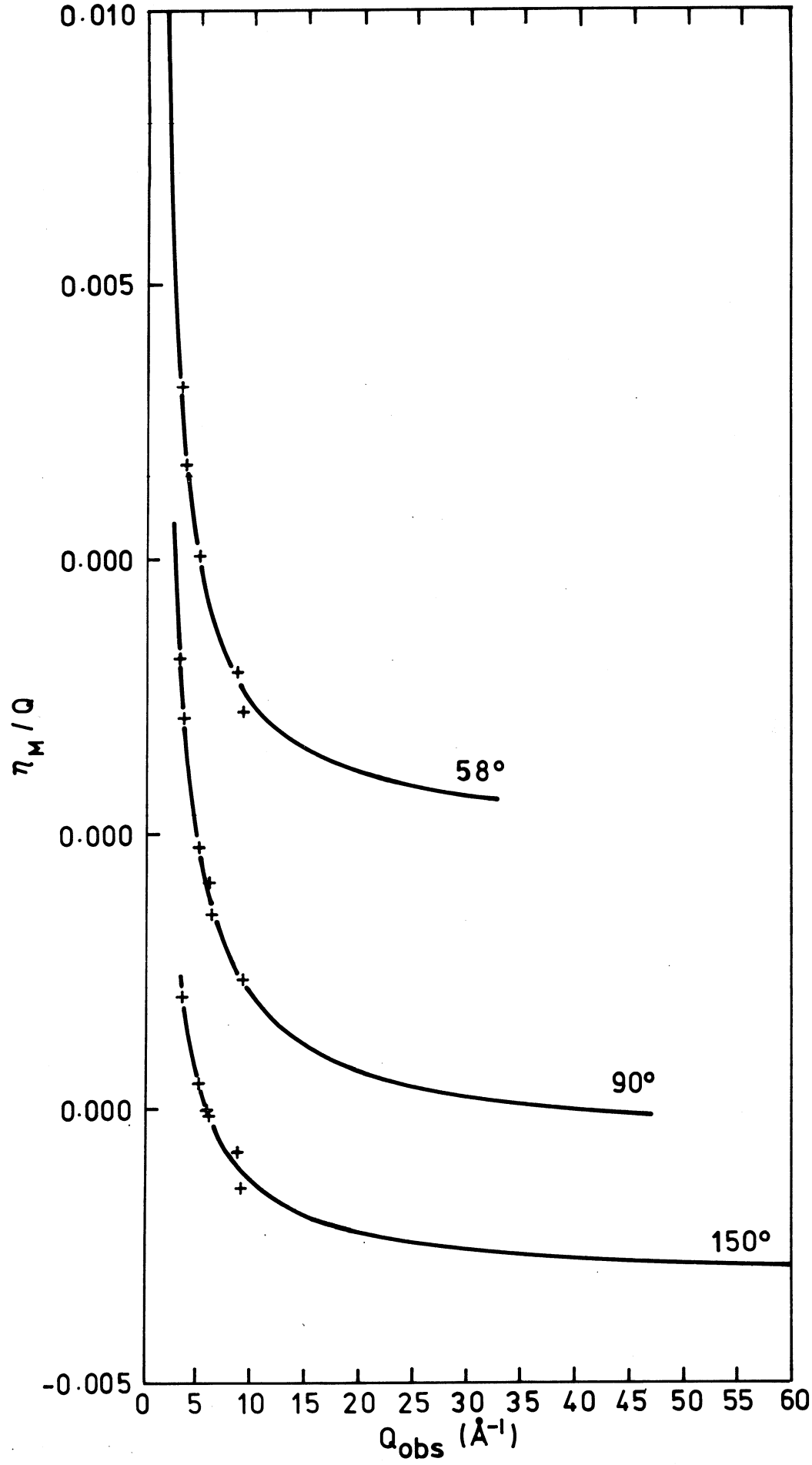

AERE - R 8925 FIG. 6

PLOT OF η_M / Q AGAINST Q_{obs}

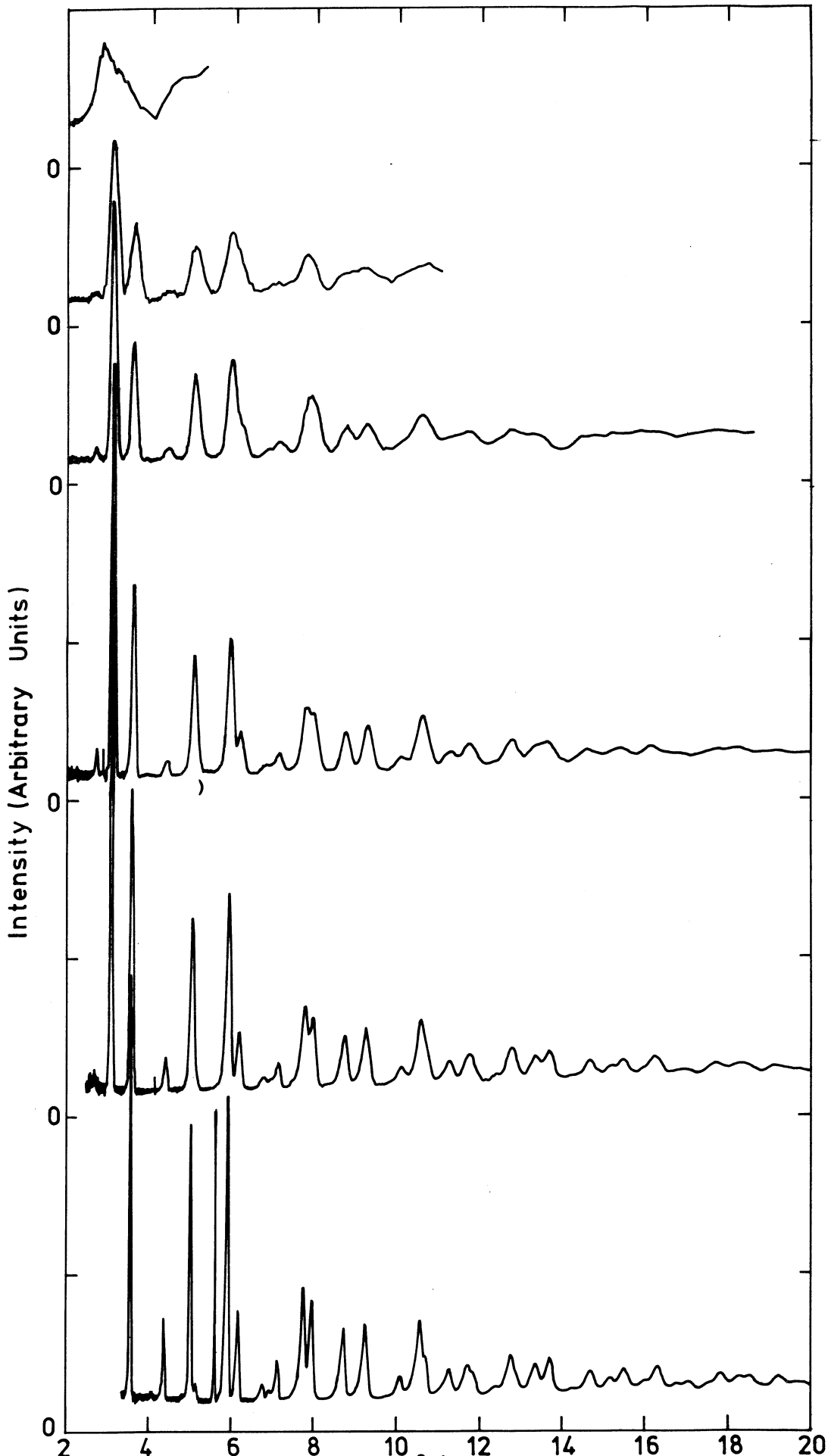

AERE-R8925 FIG.7

COMPOSITE PLOT OF THE NICKEL POWDER PATTERNS ON A Q SCALE